Polystyrene thin films in CO_2

Luciana Meli, Joseph Q. Pham, Keith P. Johnston, and Peter F. Green
Department of Chemical Engineering and Texas Material Institute, The University of Texas at Austin, Austin, Texas 78712, USA
(Received 29 July 2003; revised manuscript received 28 January 2004; published 4 May 2004)

In air, or vacuum environments, liquid polystyrene (PS) thin films (thickness, $h<100$ nm) supported by SiO_x/Si substrates are structurally metastable or unstable, depending on film thickness. They rupture and eventually form droplets on the SiO_x/Si substrates (dewet) due to the influence of destabilizing long-ranged van der Waals dispersion forces. We used scanning force microscopy to examine the structural stability of liquid PS films in the thickness range 5 nm$<h<$100 nm in liquid and in supercritical carbon dioxide (CO_2) environments. All films in this thickness range were metastable; holes developed throughout the films and over time these holes grew, impinged, and eventually formed droplets. The rate of destabilization is controlled by three factors: film thickness, temperature, and CO_2 pressure (which dictates CO_2 volume fraction in the films). Calculations of the effective interface potentials suggest that the energy barrier for nucleation and growth of holes in CO_2 is larger than that in air, and in the limit of vanishingly low PS volume fraction the films should be stable.

DOI: 10.1103/PhysRevE.69.051601 PACS number(s): 68.03.Cd, 68.08.−p, 68.15.+e

I. INTRODUCTION

Liquid and supercritical CO_2 processing of thin polymer films has important technological implications. Both liquid and supercritical CO_2 are known to plasticize many polymers, including polystyrene [1,2]. In lithographic processes CO_2 could function as spin-coating solvent [3] as well as a drying agent to prevent collapsing of small feature sizes in photoresist films, a problem associated with the use of organic solvents, and in the removal of etch residues from low k dielectrics [4–8]. Moreover, CO_2 is a viable nontoxic replacement for organic solvents in nanoparticle impregnation of polymers [9] and in the formation of nonporous films through foaming [10]. The density and solvent quality of supercritical carbon dioxide can be tuned markedly with only small variations in pressure and/or temperature. Thus, modest changes in the processing conditions can enable effective manipulation of the interfacial, thermodynamic, and transport properties of polymer films.

An important issue associated with the use of thin polymer films in various applications is the tendency of these films to exhibit thickness fluctuations at the surface that would eventually become unstable, and the film would "break up" into droplets, dewetting. One of the best known cases of this phenomenon involves polystyrene (PS) films supported by silicon substrates with a native oxide layer in air, or vacuum [11–16]. Numerous studies [13,15,17–23] propose that the stability, morphology, and dynamics of polymer films can be understood in terms of an excess intermolecular interaction free energy per unit area, or equivalently an effective interface potential $\Delta G(h)$ between the external interfaces (free surface and substrate). Both short- and long-range intermolecular interactions are accounted for in $\Delta G(h)$.

The short-range repulsive forces close to the solid surfaces may stem from chain adsorption and compression, and Born repulsion [24]. These forces, however, are often ill defined and are usually assigned a general analytical representation to capture the effect they have on the interface potential. Some of the most common representations of these forces are exponentially decaying functions of the thickness h or Lennard-Jones type of potentials.

In nonpolar films, the long-range forces are normally taken as dispersive van der Waals forces and as such are accounted for by the effective Hamaker constant A of the system. Hence, for a nonpolar film it is commonplace to write the interaction free energy as

$$\Delta G(h) = -A(12\pi h^2) + b/h^8, \tag{1}$$

where b is the strength of the short-range interactions. As expected from Eq. (1), the equilibrium morphology depends on the initial film thickness. For the specific situation involving PS on SiO_x/Si substrates, the form of the van der Waals contribution to the interface potential is modified to include the additional interface created by the silicon oxide layer of thickness d,

$$\Delta F(h) = -\frac{A_{\text{Air-PS-SiO}_x}}{12\pi h^2} + \frac{A_{\text{Air-PS-SiO}_x} - A_{\text{Air-PS-Si}}}{12\pi(h+d)^2}. \tag{2}$$

The excess free energy of PS films with air as surrounding medium is a combination of a long-range repulsion and an intermediate-range attraction. That is, the Hamaker constant between the film and the wettable silicon substrate is negative, signifying a long-range van der Waals repulsion. On the other hand, the positive value of the Hamaker constant between the nonwettable silicon oxide coating and polystyrene is a result of an intermediate-range van der Waals attraction [25]. The inclusion of short-range interactions, such as Born repulsion, leads to the global minimum at a finite thickness, as illustrated in Fig. 1. This scenario will produce spinodal instability at intermediate thicknesses when $\partial^2\Delta G/\partial h^2<0$. Thicker films are stable with respect to a spontaneous (spinodal) process and dewetting of the films occurs by nucleation and growth of holes.

Researchers have examined the interplay between long- and short-range forces by employing a range of strategies,

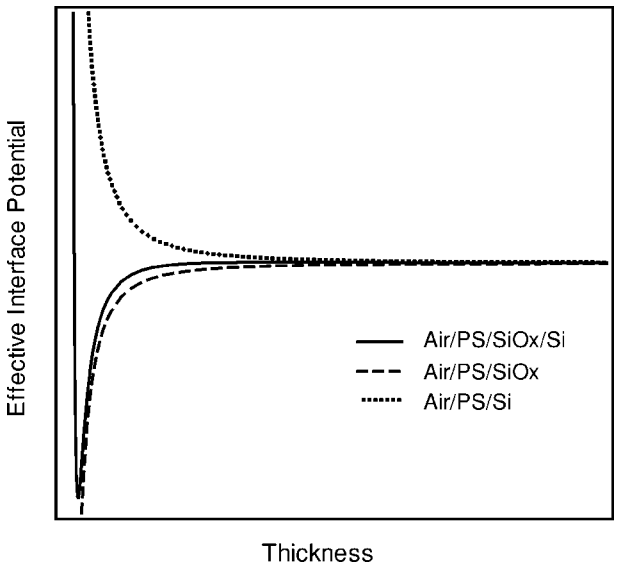

FIG. 1. Schematic of the thickness dependent effective interface potential of a PS film on an oxide covered silicon substrate, illustrating long- and short-range contributions. There is a long-range van der Waals repulsion between the substrate and PS. The dispersive attraction between silicon oxide and PS is of intermediate range when the oxide layer in the substrate is thin. A short-range repulsion near the solid surface leads to the minimum in the potential curve.

including grafting polymer molecules onto the substrate to form a brush [26], varying the thickness of native oxide layer on the substrate [27], changing the substrate [20], or replacing the medium (air) by liquids such as water or ethylene glycol [28]. In this paper we are particularly interested in the influence of a CO_2 medium on the stability of liquid PS films ($h<100$ nm) supported by SiO_x/Si substrates (CO_2/PS/SiO_x/Si).

We examined the structural stability of PS films ($5\ \text{nm}<h<100\ \text{nm}$) supported by SiO_x/Si substrates in liquid and supercritical CO_2 environments over a temperature range from 25 °C to 50 °C. The PS films, which are plasticized in this temperature range, were found to be metastable, wherein holes nucleated and increased in size. Calculations of the effective interface for the system suggest that the barrier to nucleation is higher in CO_2 than in air and at vanishingly small PS volume fractions the films should be stable. We propose that the kinetics of destabilization are controlled by three factors: film thickness, CO_2 pressure (which dictates the amount of CO_2 mixed in the film), and temperature.

II. EXPERIMENTAL SECTION

Thin films with thicknesses between 5 and 90 nm were prepared by spin-coating toluene (EM Science) solutions of polystyrene ($M_w=90\,000$, $M_w/M_n=1.04$), purchased from Pressure Chemical, onto silicon substrates (orientation 100). The silicon wafers (Wafer World Inc.) were previously cleaned by soaking in a 1:1 (w/w) methanol (EM Science)/hydrochloric acid (EM Science) solution for 30 min. Subsequently, they were rinsed with deionized water (NANOpureII, Barnstead) and dried with nitrogen gas (Matheson Gas Products, >99.999%). The wafers were then soaked in 95% sulfuric acid (Mallinckrodt, analytical grade) for 30 min, rinsed once more with deionized water and dried. The silicon substrates had a native SiO_x layer of approximately 1.7 nm as measured by spectroscopic ellipsometry (J.A. Woollam Co., Inc.). The surfaces of the films were flat and smooth, exhibiting no topographical features, when spun from solution. Prior to annealing, the polymer films were scored to expose the underlying substrate.

The samples were then loaded into a fixed volume cell, which was subsequently sealed and pressurized with carbon dioxide (Air Products, >99.999%) using a manual pressure generator (High-Pressure Equipment Co.) and heated to the desired temperature in a water bath. The pressure was controlled with a strain gauge pressure transducer (Sensotec) calibrated to within $\pm 7\times 10^{-3}$ MPa. Vitrification in these systems is determined by pressure and temperature. We note that, at the conditions studied, 25 °C, 35 °C, and 50 °C and and a CO_2 pressure of 31 MPa, all the CO_2-PS systems are in a plasticized state [1,2]. The cell was cooled to approximately 25 °C and depressurized by venting CO_2 as a vapor from the top of the cell after processing samples for a period of 120 h. In the process of depressurization and cooling, the film returns to the glassy state and the morphology of the film is frozen.

Some additional samples in the same thickness range were processed for shorter periods of time (10 and 40 h). Since it was observed that the exposure time changed the dewetting pattern (the stage of structural evolution) in samples otherwise identical, we are able to confirm that the morphology encountered is not an effect of the depressurization process.

The samples were probed with Autoprobe CP scanning force microscopy (SFM) from Park Scientific. *Ex situ* images of the surface morphologies were taken with the SFM operating in the contact mode.

Finally, contact angles were approximated by taking the radial cross section of the droplets using SFM. The contact angle measurements were obtained from the macroscopic dimensions of the droplets since local forces can distort the shape in the vicinity of the contact line [29]. Measurements of the drop radius r and height H yield the "macroscopic" contact angle using $\tan\theta/2=H/r$.

III. RESULTS

Generally, we found that ultrathin liquid PS films dewet the substrate at a much more rapid rate than thicker films in CO_2 environments, which is not unexpected. Liquid PS films of comparable thickness annealed in vacuum at 130 °C, 30 °C above the glass transition temperature, ruptured and dewetted completely over similar time scales. At higher temperatures the process was more rapid, as one would anticipate.

We now describe our data in supercritical CO_2 at 50°C. SFM images of the topographies of PS films of varying thicknesses, processed in CO_2 at $T=50$ °C for 5 days (CO_2 density of 0.88 g/cm^3), are shown in Fig. 2. Holes nucleated

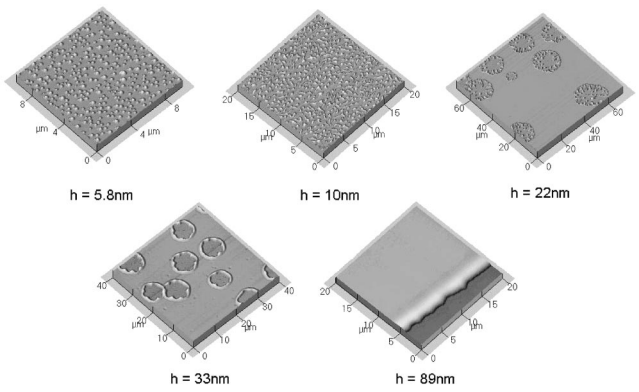

FIG. 2. Three-dimensional SFM images of the thickness dependent stability of PS films annealed in supercritical CO_2 at 50 °C and 31 MPa, after 120 h. The calculated volume fraction of CO_2 in the films is 0.14. Films of thickness $h \leqslant 33$ nm dewet the substrate. Prior to annealing, the polymer films were scored to expose the underlying substrate, as seen on the film with thickness $h = 89$ nm.

in films in the thickness range 22 nm $\leqslant h \leqslant 33$ nm, whereas the thinner films, $h \leqslant 10$ nm, completely dewet, forming droplets. On the other hand, films of $h = 89$ nm show no evidence of rupturing during this period.

Experiments conducted at $T = 35$ °C reveal qualitatively similar results, as shown by the representative topographies presented in Fig. 3. Samples of $h \geqslant 30$ nm annealed at 35 °C (CO_2 density of 0.94 g/cm^3) show no signs of rupturing after 5 days, while films of thickness $h \leqslant 21$ nm exhibited signs of dewetting during this period. Finally, with regard to PS films annealed in liquid CO_2 at a temperature of 25 °C (density of 0.97 g/cm^3), films thinner than 10 nm ruptured and dewetted, whereas thicker films remained flat and smooth after annealing for 120 h, as shown in Fig. 4.

Overall, these results indicate that the kinetics of destabilization increased with increasing temperature. Second, the thickness range of apparent kinetic stability increased with decreasing temperature.

Naively, one might interpret the former statement as an obvious one, namely, that the kinetics increase with thermal

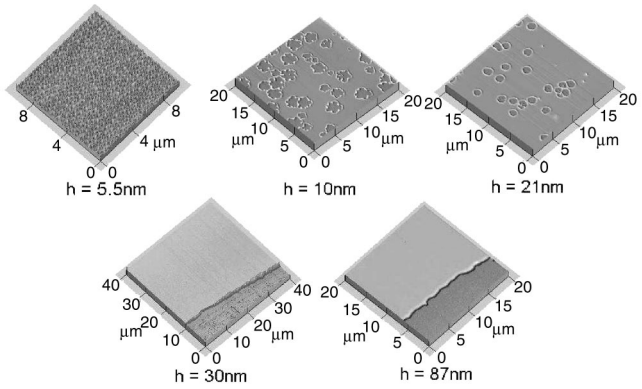

FIG. 3. SFM images of the stability of PS films in supercritical CO_2 at 35 °C and 31 MPa after 120 h. The approximate volume fraction of CO_2 in the films is 0.16. Films ruptured when $h \leqslant 21$ nm. Thicker films, $h \geqslant 30$ nm, showed only the score made to monitor changes in thickness with respect to the bare substrate.

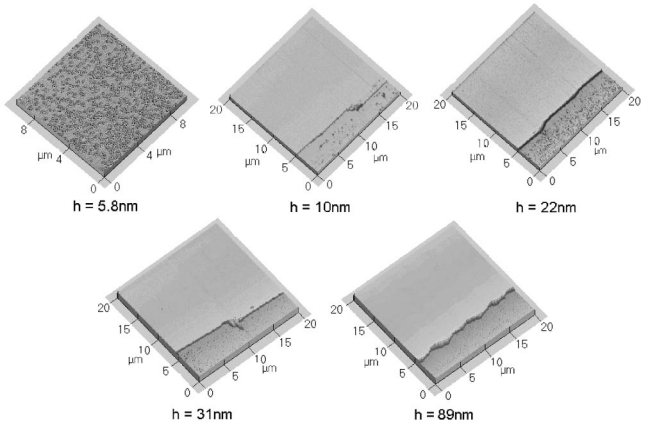

FIG. 4. SFM images of the thickness dependent stability of PS films in liquid CO_2 at 25 °C and 31 MPa after 120 h of annealing. The volume fraction of CO_2 in the films is 0.17. The thinnest film, with thickness $h = 5.8$ nm, showed hole formation. Films with thickness $h \geqslant 10$ nm showed only the score made prior to annealing.

energy, k_BT. However, there are three other factors to consider.

The PS films are plasticized by CO_2 and the CO_2 solubility increases with decreasing temperature. In fact, the CO_2 compressibility is a maximum near 35 °C.

Moreover, this phenomenon is film thickness dependent, where the effect of plasticization increases with decreasing film thickness.

The shape of the effective interface potential is influenced by CO_2 volume fraction, and as we show later, as the CO_2 volume fraction approaches 1, the system should become thermodynamically stable.

In the following section, we calculate the effective interface potential for these systems and discuss the issues of wetting of PS on SiO_x/Si substrates in air/vacuum and in CO_2 environments. We subsequently discuss the issue of thickness and temperature dependence of the kinetics.

A. Calculations of the effective interface potential

The van der Waals free energy of interaction per unit area for the three interface system CO_2/PS/SiO_2/Si has the same functional form of Eq. (2), but with Hamaker constants of the film on the oxide layer and on the substrate, $A_{CO_2\text{-}PS'\text{-}SiO_x}$ and $A_{CO_2\text{-}PS'\text{-}Si}$, respectively,

$$\Delta F(h) = -\frac{A_{CO_2-PS'-SiO_x}}{12\pi h^2} + \frac{A_{CO_2-PS'-SiO_x} - A_{CO_2-PS'-Si}}{12\pi(h+d)^2}. \tag{3}$$

The prime on PS indicates that the sorption of carbon dioxide within the film is considered in the calculation of both constants.

The following combining relation was used to calculate these nonretarded Hamaker constants:

$$A_{132} \approx (\sqrt{A_{11}} - \sqrt{A_{33}})(\sqrt{A_{22}} - \sqrt{A_{33}}). \quad (4)$$

The values taken for the silicon and silicon oxide constants, $A_{\text{Si-Si}} = 21.1 \times 10^{-20}$ J and $A_{\text{SiO}x\text{-SiO}x} = 5 \times 10^{-20}$ J, agree well with experimental measurements reported in literature [15,30,31]. For the CO_2 phase, and the CO_2-filled PS phase, we used a simplification of the Lifshitz theory through which the Hamaker constants of two identical macroscopic phases interacting across vacuum are given by [31],

$$A_{11} = 3/4kT\left(\frac{\varepsilon_1 - 1}{\varepsilon_1 + 1}\right)^2 + \frac{3h\nu_e}{16\sqrt{2}}\frac{(n_1^2 - 1)^2}{(n_1^2 + 1)^{3/2}}. \quad (5)$$

The dielectric constants are 2.55 for PS [32], 1.518 for CO_2 at 31 MPa and 50 °C, and 1.570 for CO_2 at 31 MPa and 25 °C [33]. The refractive indices are 1.557 for PS [32], 1.228 for CO_2 at 31 MPa and 50 °C, and 1.207 for CO_2 at 31 MPa and 25 °C [34]. The Lorentz-Lorentz mixing rule was used to calculate the refractive indices of the CO_2/PS mixtures from the pure component indices, assuming ideal mixing,

$$\frac{(n_{\text{mix}} - 1)^2}{(n_{\text{mix}} + 2)^2} = \sum \phi_i \frac{(n_i - 1)^2}{(n_i + 2)^2}, \quad (6)$$

where n_i is the refractive index and ϕ_i is the volume fraction of component i.

For the purposes of our calculation, we will assume that the concentration of CO_2 in the film is uniform. This is not an unreasonable assumption since any excess CO_2 in the vicinity of the interfaces occupies a very narrow region of thickness ($\sim$1 nm) compared to the film thickness. The ideal mixing assumption mentioned before is not entirely accurate since volume changes of a few percent are expected in these systems. However, the influence of the volume expansion on the value of the effective Hamaker constant should be a second order effect. The volume fraction of CO_2 was estimated to be approximately 0.14, 0.16, and 0.17, at 50 °C, 35 °C, and 25 °C, respectively, in each film [35].

The refractive indices of the 14 vol % and 17 vol % CO_2/PS mixtures were 1.518 and 1.511, respectively. By replacing n with $\varepsilon^{1/2}$ in the mixing rule expression, we estimated the dielectric constant of the mixtures to be 2.419 at 50 °C, and 2.397 at 25 °C. With the dielectric constants and refractive indices of all the phases in each system, we were in a position to compute their respective Hamaker constants with Eq. (5). Thus, the system at 50 °C and 31 MPa has $A_{\text{CO}_2\text{-CO}_2} = 1.44 \times 10^{-20}$ J and $A_{\text{PS}'\text{-PS}'} = 7.52 \times 10^{-20}$ J, while the system at 25 °C and the same pressure has $A_{\text{CO}_2\text{-CO}_2} = 1.73 \times 10^{-20}$ J and $A_{\text{PS}'\text{-PS}'} = 7.35 \times 10^{-20}$ J. These constants, along with Eq. (4), allowed us to obtain the long-range contribution to the interface potential. At this point, it is important to note that the Hamaker constants were also calculated using the complete Lifshitz theory by constructing the dielectric response function of each material using refractive index versus. wavelength data. This procedure yielded similar results as the one described above.

The repulsive interactions that prevent divergence of the dispersive forces when h approaches zero were modeled with a Born-like repulsion term $\Delta G = \Delta F + b/h^8$. The constant b of the short-range contribution was estimated by measuring contact angles of PS on the substrate. That is, with the surface tension of the polymer, we obtained the values of the free energy at the thicknesses where the minima lie by using the extended Young-Dupré equation [36]:

$$\cos\ \theta = 1 + \frac{\Delta G(h_{\text{min}})}{\gamma_{lv}} \quad (7)$$

Then, we adjusted the value of b such that the value of the minimum, $\Delta G(h_{\text{min}})$, as obtained from minimizing the Gibbs free energy expression, matched the value calculated with Eq. (7).

The measured contact angle of PS above T_g was 28.5±2°, over a temperature range of 140 –180 °C. For films annealed in CO_2 at 35 °C the average contact angle was 47°±3°, while at 50 °C it was 45°±4° (in the case of PS films annealed in CO_2 at 25 °C it was not possible to measure contact angles, since no droplet formation was observed in any sample). This means that there was no appreciable change in the contact angle between the two temperatures within experimental error. Consequently, the contact angle for the calculation of the depth of the minima in all CO_2/PS/SiO_x/Si systems was fixed to a value of 46°. It is noteworthy that the contact angle of PS droplets in CO_2 is considerably higher than that in air, indicating that the wettability of polystyrene on SiO_x/Si substrates decreases in CO_2. This statement also confirms the notion that the stability of the thick PS films in CO_2 must be dictated by the dispersive properties of the substrate, regardless of the short-range interactions with the substrate.

IV. DISCUSSION

The effective interface potential curves predicted by the calculations are presented in Fig. 5. As in the case of liquid PS in air, the curves for the CO_2/PS′/SiO_x/Si systems at 50 °C and 25 °C describe metastable films that result from a combination of dispersive long-range repulsion with shorter-range attraction. However, in the case of PS in CO_2, the curves shift to smaller values of h as the CO_2 content in the film is increased. We also observe that the magnitudes of the maxima in the potential curves of PS in CO_2 environments are greater than that of PS in vacuum. As the height of the maxima rises with increasing CO_2 content, a higher barrier to nucleation will be established that effectively opposes dewetting of the films. Furthermore, the shifts in the effective interface potential curves imply that spinodal stability ($\partial^2 \Delta G/\partial h^2 > 0$) of the PS films should be achieved in thinner regimes when CO_2 acts as a bounding fluid, as illustrated in Fig. 6. Unfortunately, we were unable to confirm this observation experimentally, since the films that would lie in the spinodal regimes are too thin to form smooth, continuous, films when spun from solution.

It is important to mention that a wetting layer was experimentally observed in all CO_2/PS′/SiO_x/Si systems as seen in Fig. 7, which confirms the existence of a minimum in the interface potential. Its thickness, however, is larger than the value of h_{min} predicted by the calculations.

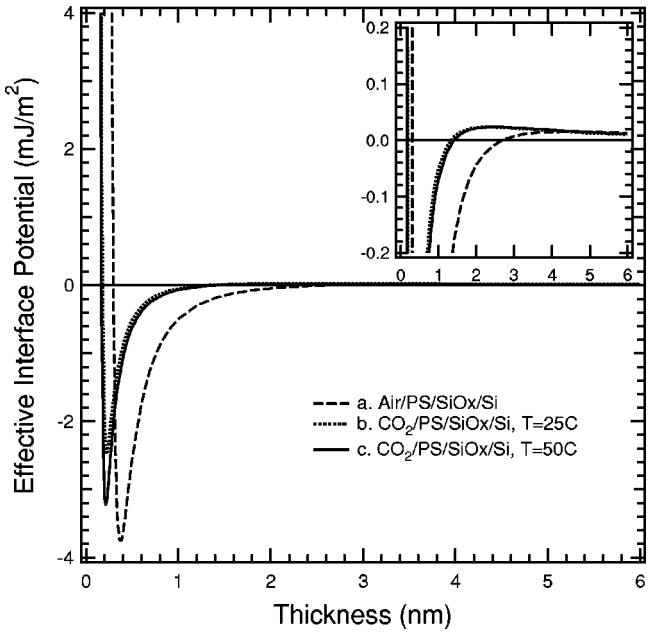

FIG. 5. The calculated effective interface potential as a function of film thickness for a model PS film in silicon substrate with a native oxide layer of thickness $d=1.7$ nm. Curve (a) represents the case where the bounding fluid is air: $A_{\text{Air-PS-Si}}=-4.87\times10^{-20}$ J, $A_{\text{Air-PS-SiO}_x}=2.93\times10^{-20}$ J, $\gamma_{\text{PS-Air}}=31$ mJ/m^2, $\theta=28.5°$. In curve (b) the bounding fluid is liquid CO_2 at $T=25$ °C and $P=31$ MPa: $A_{\text{CO}_2\text{-PS}'\text{-Si}}=-2.78\times10^{-20}$ J, $A_{\text{CO}_2\text{-PS}'\text{-SiO}x}=6.63\times10^{-21}$ J, $\phi=0.17$, $\gamma_{\text{PS-CO}_2}$[41]$=8$ mJ/m^2, $\theta=46°$. Curve (c) has supercritical CO2 at $T=50$ °C and $P=31$ MPa: $A_{\text{CO}_2\text{-PS}'\text{-Si}}=-3.02\times10^{-20}$ J, $A_{\text{CO}_2\text{-PS}'\text{-SiO}_x}=7.81\times10^{-21}$ J, $\phi=0.14$, $\gamma_{\text{PS-CO}_2}$[41]$=10.5$ mJ/m^2, $\theta=46°$. The inset presents an enlarged view at small potentials.

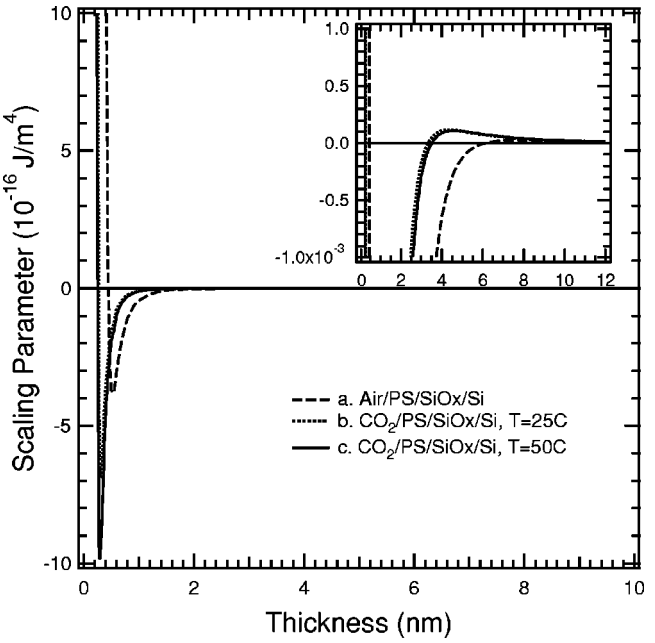

FIG. 6. Second derivative of the effective interface potential with respect to film thickness for a PS film on a silicon substrate. The parameters used to calculate each curve are presented in caption in Fig. 5.

Qualitatively, the model suggests that the barrier to nucleation of holes in PS films in the CO_2 environments is larger than that in atmospheric environments. In fact, further increases in the CO_2 content of the film, achieved by increasing the pressure or decreasing the temperature, have the effect of increasing the magnitude of the maximum (barrier) in the interface potential. In the limiting case where the volume fraction of PS is negligible, we would effectively have a layer of pure CO_2. Since the Hamaker constant of a $Si/SiO_x/CO_2$ system is negative for a wide range of processing conditions, one would expect stability of the CO_2 layer. Therefore, in principle, one could achieve complete thermodynamic stability if the uptake of carbon dioxide reaches a critical value where $A_{\text{Air-PS}'\text{-SiO}_x}$ becomes negative. However, in practice, it becomes increasingly difficult to augment the content of CO_2 because the slope of the sorption isotherms above the compressibility regime is very small [37].

The model also suggests that the behavior of the films at 25 °C and 50 °C should be similar, since in reality the difference in CO_2 absorption between the two temperatures is small (approximately 3%). That is, identical samples of a given thickness should exhibit similar morphologies at equilibrium, regardless of which temperature is chosen to anneal the films. Nevertheless, experimentally we observe an apparent increase in the structural stability of the samples in the time scale of our experiments. We are therefore led to believe that the difference in morphologies of the films at the different temperatures should be primarily related to kinetics.

In air or vacuum environments, the kinetics of destabilization should be largely dictated by two parameters: thickness, and thermal energy, k_BT. One can envision that in CO_2 environments a third parameter may come into play, namely, CO_2 pressure. More specifically, if the vitrification (liquid to glass) transition pressure is P_g then, $\Delta P-P_g$ is a key parameter for understanding the kinetics of destabilization of the films. This issue is examined in further detail below.

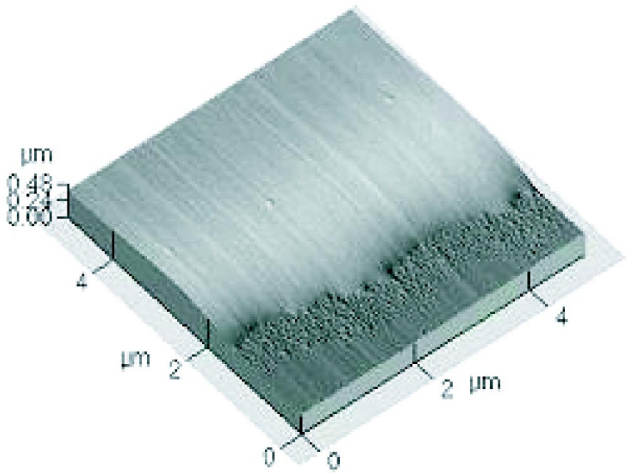

FIG. 7. 5×5 μm SFM image of a 89 nm thick film in supercritical CO_2 at 50 °C and 31 MPa, after 120 h. In the image we can discern between the bare substrate exposed by the scoring made prior to annealing, and the wetting layer that has ruptured and formed droplets.

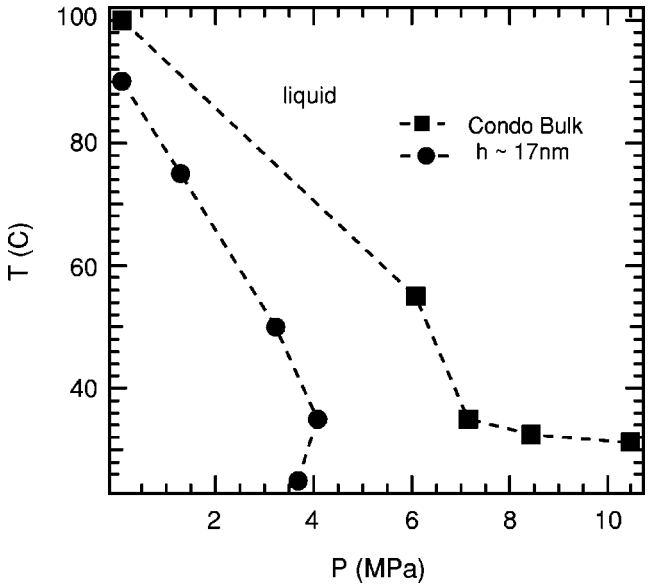

FIG. 8. Vitrification envelope for a PS thin film with a thickness of $h=17$ nm (circles) and for bulk PS (Condo and co-workers [1]) are shown here. Films outside the relevant envelope are plasticized (liquid). The lines drawn through the data are guides to the eye.

It is well established that the T_g of a polymer film exhibits a thickness dependence under atmospheric environments when the thickness is sufficiently small [38–40]. In a similar fashion, the CO_2 pressure at which devitrification of a polymer film occurs, P_g, has also been found to be thickness dependent. Specifically, it has been found that lower CO_2 pressures are required to plasticize thinner films [41]. This dependence can be rationalized in terms of the effective amount of CO_2 in the film, which is responsible for the plasticization of the polymer. For several polymers, like poly(dimethylsiloxane) (PDMS) and PS, there exists an enhancement of CO_2 sorption [42,43] in thin films due mainly to excess CO_2 at the boundaries. As the thickness of a film decreases, the effect of the boundaries on the overall content of CO_2 becomes more pronounced and a decrease of the P_g relative to the bulk can be observed.

In addition, bulk and thin film systems may exhibit atypical vitrification effects under CO_2 environments. Some polymers, like poly(methylmethacrylate) (PMMA), undergo the expected vitrification when decreasing the temperature isobarically, due to loss of configurational entropy. However, upon further cooling, they devitrify because of the increase in the solubility of CO_2 with decreasing temperature at a given pressure [1]. The phenomenon is known as retrograde vitrification, and it is characterized by a vitrification envelope below a maximum pressure on a pressure versus temperature plot, as seen in Fig. 8. It has been observed in bulk and thin film PMMA and poly(ethylmethacrylate) (PEMA), but does not occur in bulk PS. Recent experimental work, however, has shown that retrograde vitrification does indeed occur in thin film PS systems. A detailed account of these results and their implications can be found in the work of Pham [44].

In the aforementioned work, measurements of the CO_2-induced devitrification of PS were performed at different thicknesses and at isotherms of 25, 35, 50, and 75 °C. A representative curve of their data at a thickness of 17 nm is presented in Fig. 8. The P_g thickness dependence was fitted to a modified version of the empirical equation proposed by Keddie [38],

$$P_g(h) = P_{gbulk}[1 - (A/h^{\delta})], \tag{8}$$

with adjustable parameters A and δ. The equation describes the P_g versus film thickness data for PS, at our experimental isotherms and film thickness (see Table I), reasonably well.

TABLE I. To the left, the pressures at which the films become plasticized are shown for different temperatures. To the right, the pressures beyond P_g at which films are processed are shown for different temperatures.

h(nm)	P_g(MPa)			ΔP(MPa)		
	25 °C	35 °C	50 °C	25 °C	35 °C	50 °C
5.5	0.9	1.2	1.0	30.1	29.8	30.0
10	2.2	3.1	2.4	28.8	28.0	28.6
20	3.5	4.3	3.6	27.5	26.7	27.4
30	4.0	4.6	4.0	27.0	26.4	27.0
90	4.8	5.2	4.5	26.2	25.8	26.5

As mentioned before, the kinetics of destabilization of the films are determined by the CO_2 pressure, the temperature, and the film thickness. From Table I we see that ΔP decreases with increasing film thickness. Hence, in addition to the disjoining pressure, the increasing ΔP with decreasing film thickness contributes to an increase in destabilization kinetics.

It is interesting to note that there should be an enhancement of the kinetics of destabilization at lower temperatures due to the increased solubility of CO_2 at these conditions that leads to lower viscosity of the films. On the other hand, the increased solubility at lower temperatures also helps in stabilizing the films towards hole formation, as suggested by calculations. Despite these two effects, it appears in this case that temperature has a larger impact on the destabilization kinetics, with the largest kinetics observed at the highest temperature 50 °C.

We can get some insight into the relative contributions of the effects of CO_2 volume fraction compared to that of temperature. This can be accomplished using a model developed by Chow [45] to predict the depression of T_g due to sorption by a gas. The model predicts that

$$\ln\left[\frac{T_g}{T_g(w_{CO_2}=0)}\right] = \beta[(1-\theta)\ln(1-\theta) + \theta \ln \theta],$$

$$\theta = \alpha\left[\frac{w_{CO_2}}{1-w_{CO_2}}\right], \tag{9}$$

where w_{CO_2} is the weight fraction of CO_2, and parameters β and α are constants that depend on the polymer and the gas. Values of β and α used to calculate the T_g depression were taken from the literature [46] ($\beta=0.635$ and $\alpha=0.972$) for

CO_2 sorption in PS. We now proceed by considering the thick films, where T_g is independent of thickness ($h \sim 90$ nm). At temperatures of 50, 35, and 25 °C the thick films should be approximately 30, 27, and 24 °C above their T_g, respectively. According to this model a thinner film, of $h=14$ nm, should be 43, 39, and 35 °C above its T_g, at 50, 35 and 25 °C, respectively. The observed increasing kinetics with increasing temperature is consistent with the notion that the effective viscosities should decrease as the temperature increases above the T_g.

It is clear from the aforementioned that PS films can be processed at low temperatures compared to those required for processing in air. In fact, to achieve the same conditions in air (or vacuum), our estimates suggest that the experiments would have to be conducted between 130 °C and 140°C, where they are at comparable temperature differences above their T_g's.

V. CONCLUSIONS

We showed that thin liquid PS films ($h<100$ nm) supported by SiO_x/Si substrates in liquid and in supercritical CO_2 environments are metastable. Holes nucleate throughout the films, grow, and eventually form droplets on the substrate. The contact angle of the PS droplets in CO_2 environments was found to be significantly higher than that of PS droplets in air, indicating a decrease in the wetting tendency of the polymer on the substrate in CO_2 environments. Estimates of the effective interface potentials suggest that a higher barrier to nucleation exists in the CO_2 environments than in air. In fact, at vanishingly small PS volume fractions in the films, the film should become stable.

In air, increasing the thermal energy of a system results in increased kinetics of destabilization. However, in liquid and in supercritical CO_2 environments, competing factors control destabilization of the film. The decreased CO_2 solubility at high temperatures causes slower destabilization kinetics, but augments the stability of the film because of an increase in the effective barrier to nucleation. On the other hand, increases in thermal energy lead to faster kinetics as the viscosity of the film decreases. Thus, there is a delicate interplay between effects due to CO_2 sorption, and those due to temperature. In this case the effects of temperature control the kinetics of destabilization of the PS films.

In any event, it is clear that the morphological structures observed in CO_2 are similar to those in air. However, the main advantage of processing PS in CO_2 that films can be processed at much lower temperatures with similar results.

ACKNOWLEDGMENTS

This work was supported by the National Science Foundation under Grant Nos. CHE-9876674 and DMR 0072809 and by the Robert A. Welch Foundation.

[1] P. D. Condo, D. R. Paul, and K. P. Johnston, Macromolecules **27**, 365 (1994).
[2] R. G. Wissinger and M. E. Paulaitis, J. Polym. Sci., Part B: Polym. Phys. **29**, 631 (1991).
[3] B. J. Novick, R. G. Carbonell, and J. M. DeSimone, Polym. Mater. Sci. Eng. **84**, 51 (2001).
[4] S. G. Kazarian, Polym. Sci., Ser. C **41**, 78 (2000).
[5] X. Zhang , J. Vac. Sci. Technol. B **21**, 2590 (2003).
[6] H. Namatsu, J. Vac. Sci. Technol. B **19**, 2709 (2001).
[7] C. M. Stafford, T. P. Russell, and T. J. McCarthy, Macromolecules **32**, 7610 (1999).
[8] D. L. Goldfarb , J. Vac. Sci. Technol. B **18**, 3313 (2000).
[9] H. Liu and M. Z. Yates, Langmuir **18**, 6066 (2002).
[10] S. K. Goel and E. J. Beckman, AIChE J. **41**, 357 (1995).
[11] R. Seeman, S. Herminghaus, and K. Jacobs, J. Phys.: Condens. Matter **13**, 4925 (2001).
[12] G. Reiter, Phys. Rev. Lett. **68**, 75 (1991).
[13] K. Jacobs and S. Herminghaus, Langmuir **14**, 965 (1998).
[14] J. A. Forrest, Eur. Phys. J. E **8**, 261 (2002).
[15] P. Muller-Buschbaum , Europhys. Lett. **40**, 665 (1997).
[16] J. L. Masson, O. Olufokunbi, and P. F. Green, Macromolecules **35**, 6992 (2002).
[17] F. Brochard-Wyart and J. Daillant, Can. J. Phys. **68**, 1084 (1990).
[18] G. Reiter, Phys. Rev. Lett. **81**, 75 (1992).
[19] P. G. deGennes, Rev. Mod. Phys. **57**, 827 (1985).
[20] R. Limary, P. F. Green, and K. R. Shull, Eur. Phys. J. E **8**, 103 (2002).
[21] A. Sharma, Langmuir **9**, 861 (1993).
[22] A. Sharma, Langmuir **9**, 3580 (1993).
[23] M. P. Valignat , Fluid Phase Equilib. **150-151**, 615 (1998).
[24] K. Kargupta, R. Konnur, and A. Sharma, Langmuir **16**, 10 243 (2000).
[25] K. Kagrupta and A. Sharma, J. Colloid Interface Sci. **245**, 99 (2002).
[26] G. Reiter , Europhys. Lett. **46**, 512 (1999).
[27] R. Seeman, S. Herminghaus, and K. Jacobs, Phys. Rev. Lett. **86**, 5534 (2001).
[28] G. Reiter , Langmuir **15**, 2551 (1999).
[29] E. Vitt and K. R. Shull, Macromolecules **28**, 6349 (1995).
[30] J. Visser, Adv. Colloid Interface Sci. **3**, 331 (1972).
[31] J. N. Israelachvili, *Intermolecular and Surface Forces* (Academic Press, New York, 1992)
[32] D. B. Hough and L. R. White, Adv. Colloid Interface Sci. **14**, 3 (1980).
[33] M. Hourri, J. M. St-Arnaud, and T. K. Boser, J. Chem. Phys. **106**, 1780 (1997).
[34] A. Michels and J. Hamers, Physica IV **10**, 995 (1937).
[35] K. Lee and I. C. Sanchez (private communication)
[36] A. Sharma, Langmuir **14**, 4915 (1998).
[37] P. D. Condo, I. C. Sanchez, and K. P. Johnston, Macromolecules **25**, 6128 (1992).
[38] J. L. Keddie, R. A. Jones, and R. A. Cory, Europhys. Lett. **27**, 59 (1994).
[39] J. Q. Pham and P. F. Green, J. Chem. Phys. **116**, 5801 (2002).
[40] J. Q. Pham and P. F. Green, Macromolecules **36**, 1665 (2003).

[41] J. Q. Pham , Phys. Rev. Lett. **91**, 175503 (2003).
[42] S. M. Sirard , Macromolecules **36**, 3365 (2003).
[43] T. Koga , Europhys. Lett. **60**, 559 (2002).
[44] J. Pham, P. F. Green, and K. P. Johnston, J. Phys. Chem. B **108**, 3457 (2004).
[45] T. S. Chow, Macromolecules **13**, 362 (1980).
[46] R. R. Gupta , Macromolecules **36**, 346 (2003).